Nematodynamics of anisotropic liquid crystals using a singular potential

Lucas Myers

November 15, 2022

1 Introduction

Nematic liquid crystals constitute an interesting phase between crystals and typical fluids because they exhibit orientational order, but lack translational order. Thus their molecules tend to orient themselves along the same axis for thermodynamic reasons, but their evolution is also mediated by flows throughout the system. Further, topological defects can arise when molecular orientations wrap around points or lines in nontrivial ways. It is a considerable challenge to properly couple both the thermodynamic effects of alignment with the hydrodynamic flow effects, especially when the topological nature of defects makes it necessary to introduce a tensor-valued order parameter to keep track of the liquid crystal state. Here we describe one of the previously-proposed hydrodynamic models, and adjust the bulk free energy so that the model can describe anisotropic elasticity – that is, a system in which different types of molecular distortions are preferred differently by the system.

To begin, we give an introduction to liquid crystal theory, first in the equilibrium case and then in the non-equilibrium case describing both the typical Landau-de Gennes free energy, and then an extension to the somewhat lesser-used Maier-Saupe mean-field free energy. This mean-field theory is what allows us to include anisotropic elasticity in our model, and thus explore associated effects such as dynamics arising from altered defect morphology. As we will show, a minimal Landau-de Gennes bulk free energy is not bounded below when anisotropy is included, and so can cause simulated configurations to diverge. After this we introduce the hydrodynamic model, and subsequently show the computational scheme which is used to solve the model. To establish the efficacy of our code, we compare configurations prepared by our computational scheme to other, previously-established results. Finally, we indicate some of the systems and phenomena which we hope to investigate with our model.

2 Equilibrium liquid crystal theory

2.1 The Q-tensor

The systems that we will be concerned with display a nematic liquid crystal phase. The phrase "liquid crystal" indicates that the molecules lack positional order like a liquid, but they have strong orientational order like a crystal. Put another way, the molecules are able to move around one another with relative ease, but they tend to align along some preferred direction. To display this kind of aligning behavior, the molecules in question must be anisotropic in some way. In Fig. 1, the molecule is completely anisotropic and so we may assign a vector roughly along its longest axis, and pointing in some particular direction (here we choose towards the benzene rings, but we could have just as easily chosen towards the tail).
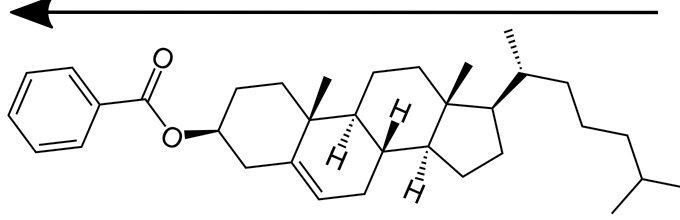
Figure 1: A cholesteryl benzoate molecule, along with an arrow representing a unit vector which we use to characterize its orientation. Image from [1]

Two phases can be distinguished: the isotropic phase given in Fig. 2a in which molecules are randomly oriented, and the nematic phase given in Fig. 2b in which the molecules are oriented along some particular axis, but not necessarily in the same direction. To encode information from
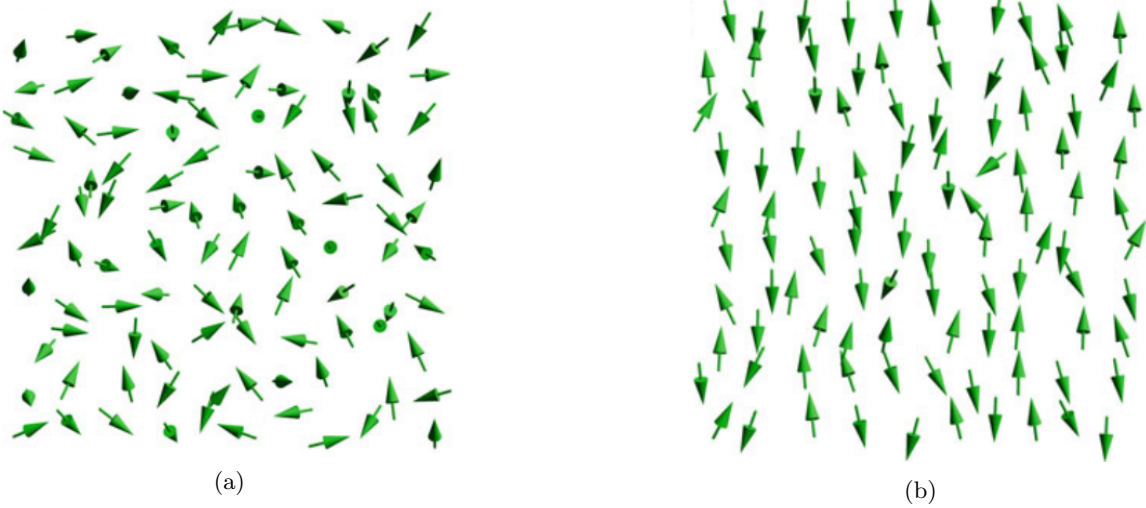

(a)

(b)

Figure 2: Schematic representation of (a) isotropic and (b) nematic alignment patterns of molecules. Cartoons from [2]

the system about the phase, a tensorial order parameter Q is defined in terms of an average over all of the molecular orientations $\mathbf{p}$:

$$Q = \langle \mathbf{p} \otimes \mathbf{p} \rangle - \tfrac{1}{3}I \tag{1}$$

with I the 3×3 identity matrix. Note that this quantity is even in $\mathbf{p}$ because, in the aggregate molecules with orientation $\mathbf{p}$ and $-\mathbf{p}$ should be treated equally. Note also that this quantity is symmetric and traceless, where the latter follows because $\mathbf{p}$ is a unit vector. Finally, we remark that the largest possible eigenvalue of Q is $\tfrac{2}{3}$ while the most negative possible eigenvalue is $-\tfrac{1}{3}$. Both are achieved when $\mathbf{p}$ always points directly along some particular axis. This condition for Q representing a physical state becomes important when we consider nonequilibrium systems.

To interpret this quantity physically, note that we may diagonalize the tensor into an orthonormal eigenbasis with eigenvalues $\{q_1, q_2, -(q_1+q_2)\}$ and corresponding eigenvectors $\{\mathbf{n}, \mathbf{m}, \mathbf{l}\}$:

$$\begin{aligned} Q &= q_1(\mathbf{n} \otimes \mathbf{n}) + q_2(\mathbf{m} \otimes \mathbf{m}) - (q_1 + q_2)(\mathbf{l} \otimes \mathbf{l}) \\ &= S(\mathbf{n} \otimes \mathbf{n} - \tfrac{1}{3}I) + P(\mathbf{m} \otimes \mathbf{m} - \mathbf{l} \otimes \mathbf{l}) \end{aligned} \tag{2}$$

where we have used the fact that $\{\mathbf{n}, \mathbf{m}, \mathbf{l}\}$ form an orthonormal basis so that $\mathbf{n} \otimes \mathbf{n} + \mathbf{m} \otimes \mathbf{m} + \mathbf{l} \otimes \mathbf{l} = I$ which is basis independent, and we have defined $S = \tfrac{3}{2}q_1$ and $P = \tfrac{1}{2}(q_1 + q_2)$. Here S and P are independent parameters, $\mathbf{n}$ is defined by a polar angle and an azimuthal angle, $\mathbf{m}$ is defined by a

single angle in the plane perpendicular to **n**, and **l** is completely determined. Hence, we have five degrees of freedom which matches what we would expect from a 3×3 traceless symmetric tensor.

If we consider Eq. (1), for a set of particles that are uniformly distributed in the azimuthal direction about a main axis **n**, then we may write each molecule as:

$$\mathbf{p} = \cos\phi \sin\theta \, \mathbf{m} + \sin\phi \sin\theta \, \mathbf{l} + \cos\theta \, \mathbf{n} \tag{3}$$

We call these types of systems "uniaxial" because the molecules point mainly along one axis. If we calculate Q, we get:

$$Q = \left\langle \cos^2\theta - \tfrac{1}{3} \right\rangle \mathbf{n} \otimes \mathbf{n} - \tfrac{1}{2} \left\langle \cos^2\theta - \tfrac{1}{3} \right\rangle \mathbf{m} \otimes \mathbf{m} - \tfrac{1}{2} \left\langle \cos^2\theta - \tfrac{1}{3} \right\rangle \mathbf{l} \otimes \mathbf{l} \tag{4}$$

where any term with $\cos\phi$ or $\sin\phi$ has gone to zero, and any term with $\sin^2\phi$ or $\cos^2\phi$ has gone to $\tfrac{1}{2}$. Now we may simply read off the eigenvalues of Q to find that:

$$S = \tfrac{3}{2} \langle \cos^2\theta - \tfrac{1}{3} \rangle = \langle P_2(\cos\theta) \rangle \tag{5}$$

where P_2 is the second Legendre polynomial. Hence, if $S = 1$ we have that $\theta = 0$ always which corresponds to perfect alignment. Otherwise, if θ is uniformly distributed we have that $S = 0$. Thus, S characterizes the degree of alignment and **n** – sometimes called the "director" – characterizes the direction of alignment in uniaxial nematics. Indeed, historically the development of liquid crystal theory has used the director and scalar order parameter S to describe the evolution of nematic systems [3, 4].

2.2 Landau-de Gennes free energy

To predict the equilibrium configuration of a liquid crystal system, we must first write down a free energy as a function of the order parameter, and then find the order parameter value which minimizes this free energy. As a first approach, we recount the method elucidated by Landau and applied to nematic liquid crystal systems by de Gennes. This is done by first assuming that the free energy is a smooth function, and then Taylor expanding in the appropriate order parameter, in this case the Q-tensor. Additionally, we only keep terms which obey the symmetry of the system. For us, these are terms which can undergo an arbitrary rotation, given that the direction of alignment will correspond to a broken symmetry when the phase transition is from the isotropic state to the nematic state.

Given that we have a tensor-valued order parameter, the terms which are unchanged by rotations are all of the possible ways the Q-tensor can be contracted to get a scalar value. In order to see a first-order phase transition from isotropic to nematic phases, one must expand up to fourth order in Q:

$$F(Q) = \frac{1}{2}A(Q:Q) + \frac{1}{3}B(QQ):Q + \frac{1}{4}C_1(Q:Q)^2 + \frac{1}{8}C_2(QQ):(QQ) \tag{6}$$

where here juxtaposition means standard matrix multiplication $QQ \to Q_{ik}Q_{kj}$, and dots indicate contraction over indices from innermost to outermost $Q:Q \to Q_{ij}Q_{ji}$. A, B, C_1, and C_2 are all empirical quantities. Note that:

$$(Q:Q)^2 = 2(QQ):(QQ) \tag{7}$$

which can be seen most easily by choosing a basis wherein Q is diagonal (both quantities are scalar and are therefore unchanged by rotations), and then explicitly calculating the contractions. Given this, we can define $C = (C_1 + \tfrac{1}{2}C_2)$ to get only three terms in our free energy:

$$F(Q) = \frac{1}{2}A(Q:Q) + \frac{1}{3}B(QQ):Q + \frac{1}{4}C(Q:Q)^2 \tag{8}$$

(a) Landau-de Gennes bulk free energy
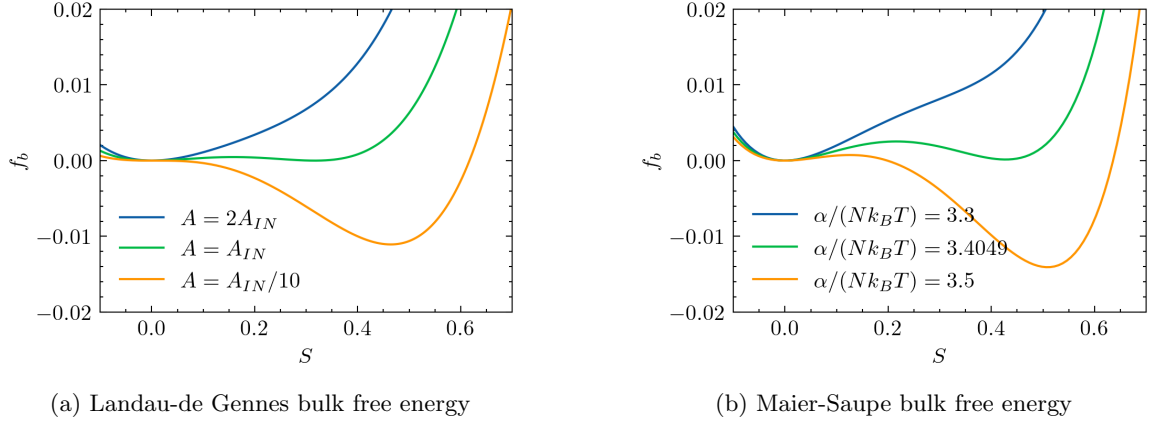

(b) Maier-Saupe bulk free energy

Figure 3: Landau-de Gennes and Maier-Saupe bulk free energies as a function of the scalar order parameter S for a uniaxial system. For LdG we vary the A parameter in terms of A_{IN}, and for MS we vary α/Nk_BT around 3.4049, both being the value at which the isotropic-nematic transition occurs.

For a uniaxial nematic ($P = 0$) the free energy only depends on the scalar order parameter S, given that it must be insensitive to rotations. A is typically taken to be linear in temperature for thermotropic liquid crystals $A = a(T - T_0)$ with T_0 some reference temperature, and so we plot the free energy for several values of A which corresponds to several temperatures in Fig. 3a.

At low temperatures, the global minimum is at $S \neq 0$ so that the system is in a nematic state, whereas at high temperatures the global minimum is at $S = 0$, the isotropic state. There is a cross-over at $A = A_{IN}$ at which point we have coexistence between isotropic and nematic phases. Thus, the theory correctly predicts a phase change, supposing that the empirical parameters have the correct signs.

2.3   Maier-Saupe mean-field energy

While the Landau approach works for many systems, and is rather powerful given its relative simplicity, we seek a theory which is more grounded in the microscopic details of the system. This will allow us to write a theory which has far fewer undetermined factors such as the A, B, C of Landau-de Gennes, as well as avoid some pitfalls when we venture into nonequilibrium thermodynamics in Sec. 3.

To begin, we write down an energy corresponding to the nematic system which will then help us write down a free energy. Rather than trying to enumerate the average energy from pairwise interactions between particles, we make a mean-field approximation whereby each molecule interacts with an effective potential produced by all other molecules. In this way, we can uncouple fluctuations of individual molecules, and thus neglect correlations between their orientations.

To start, we assume that the pair-wise particle energy of the liquid crystal molecules is only dependent on relative angle γ get:

$$U = -JP_2\cos(\gamma) = -J\left[\frac{3}{2}\cos^2(\gamma) - \frac{1}{2}\right] \tag{9}$$

Here $J > 0$ so that the energy is minimized when γ is a multiple of π (i.e. the particles are aligned or antialigned). One may derive this potential in any number of ways, including a quantum mechanical calculation of the dipole interactions between particles, an excluded volume calculation by treating the particles as cylinders, or by taking the pairwise energy as an arbitrary function of orientation and expanding in spherical harmonics.

4

In any case, we may calculate for particles with orientations $\mathbf{p}$ and $\mathbf{q}$ that:

$$\langle\cos^2(\gamma)\rangle = \langle(\mathbf{p}\cdot\mathbf{q})(\mathbf{p}\cdot\mathbf{q})\rangle = \langle(\mathbf{p}\otimes\mathbf{p}):(\mathbf{q}\otimes\mathbf{q})\rangle \approx \langle\mathbf{p}\otimes\mathbf{p}\rangle:\langle\mathbf{q}\otimes\mathbf{q}\rangle \tag{10}$$

where in the last line we have used the mean-field theory that each molecule only interacts with an effective field from the other molecules, and so fluctuations in $\mathbf{p}$ should be independent of fluctuations in $\mathbf{q}$. Using this along with the definition of Q, we obtain that the average energy of the entire system by:

$$\langle E\rangle = -\alpha\, Q : Q \tag{11}$$

with $\alpha = \frac{1}{3}NqJ$ where N is the number of molecules, and q is the number of neighbors that each particle interacts with.

Now that we have an energy as a function of the order parameter, we must write down a free energy. This is done in the usual way, using the definition of the free energy in terms of the entropy:

$$F = \langle E\rangle - TS \tag{12}$$

where

$$S = -Nk_B \int_{S^2} \rho(\mathbf{p})\log\left(4\pi\rho(\mathbf{p})\right)dS(\mathbf{p}) \tag{13}$$

where the probability distribution function $\rho(\mathbf{p})$ describes the probability that a particular molecule be pointing in some direction given by a point $\mathbf{p}$ on the unit sphere S^2, N is the number of molecules, and dS is the surface measure of S^2. Note that, because the interaction energy only depends on the relative angle modulo π, we have that $\rho(\mathbf{p}) = \rho(-\mathbf{p})$.

We need to determine S as a function of the order parameter Q from Eq. (1):

$$Q = \int_{S^2}\left(\mathbf{p}\otimes\mathbf{p} - \tfrac{1}{3}I\right)\rho(\mathbf{p})dS(\mathbf{p}) \tag{14}$$

Given that there are many potential $\rho(\mathbf{p})$ functions which will produce a particular value for Q, we seek the one which will maximize S. This may be done via the method of Lagrange multipliers, by first fixing a value of Q and then taking (14) to be a constraint on $\rho(\mathbf{p})$. The resulting Lagrangian is given as:

$$\begin{aligned}\mathcal{L}[\rho] &= S + \Lambda : \left(\int_{S^2}\left(\mathbf{p}\otimes\mathbf{p} - \tfrac{1}{3}I\right)\rho(\mathbf{p})dS(\mathbf{p}) - Q\right) \\ &= \int_{S^2}\rho(\mathbf{p})\left(-Nk_B\log\left(4\pi\rho(\mathbf{p})\right) + \Lambda:(\mathbf{p}\otimes\mathbf{p} - \tfrac{1}{3}I)\right)dS(\mathbf{p}) - \Lambda:Q\end{aligned} \tag{15}$$

where Λ is a tensorial Lagrange multiplier. Note that Eq. (14) actually only defines five constraints, because the fixed Q will be traceless and symmetric by definition, and the integral around the sphere has a traceless and symmetric integrand regardless of $\rho(\mathbf{p})$. Hence, if $\rho(\mathbf{p})$ satisfies the five constraints corresponding to the five degrees of freedom of Q then it will necessarily satisfy the other (redundant) constraints. For the sake of finding a unique set of Lagrange multiplier values, we then take Λ to also be traceless and symmetric so that only the unique constraint equations show up in Eq. (15).

To maximize the Lagrangian, we take the variation at fixed Q, which yields:

$$\delta\mathcal{L} = \int_{S^2}\left(-Nk_B\log\left(4\pi\rho(\mathbf{p})\right) + \Lambda:(\mathbf{p}\otimes\mathbf{p} - \tfrac{1}{3}I) - Nk_B\right)\delta\rho\, dS(\mathbf{p}) \tag{16}$$

For the above to be zero for an arbitrary variation $\delta\rho$, we must have that the factor in parentheses is zero. Solving the expression for $\rho(\mathbf{p})$ yields:

$$\rho(\mathbf{p}) = \frac{1}{4\pi}\exp\left(-\left(\frac{1}{Nk_B}\frac{1}{3}\Lambda:I + 1\right)\right)\exp\left(\frac{1}{Nk_B}\Lambda:(\mathbf{p}\otimes\mathbf{p})\right) \tag{17}$$

5

We have one further restriction on $\rho(\mathbf{p})$, which is that it integrates to one. Dividing by its integral around the sphere cancels the factors out front which are constant in $\mathbf{p}$. Further, we redefine $\Lambda \to N k_B \Lambda$, so that the expression simplifies to:

$$\rho(\mathbf{p}) = \frac{\exp\left(\mathbf{p}^T \Lambda \mathbf{p}\right)}{Z[\Lambda]} \tag{18}$$

with the partition function $Z[\Lambda]$:

$$Z[\Lambda] = \int_{S^2} \exp\left(\mathbf{p}^T \Lambda \mathbf{p}\right) dS(\mathbf{p}) \tag{19}$$

Note that we have used the identity $\Lambda : (\mathbf{p} \otimes \mathbf{p}) = \mathbf{p}^T \Lambda \mathbf{p}$ which is a simple computation using Cartesian coordinates.

Given this, we may find Λ implicitly as a function of Q from Eq. (14):

$$\begin{aligned}
Q &= \frac{1}{Z} \int_{S^2} \exp(\mathbf{p}^T \Lambda \mathbf{p}) \left(\mathbf{p} \otimes \mathbf{p} - \tfrac{1}{3} I\right) dS(\mathbf{p}) \\
&= \frac{\partial \log Z}{\partial \Lambda} - \frac{1}{3} I
\end{aligned} \tag{20}$$

where we have integrated the second term using the definition of Z. Additionally, we have an explicit expression for S in terms of the Lagrange multiplier Λ:

$$\begin{aligned}
S &= -N k_B \frac{1}{Z} \int_{S^2} \exp(\mathbf{p}^T \Lambda \mathbf{p}) \left(\log 4\pi + \mathbf{p}^T \Lambda \mathbf{p} - \log Z\right) dS(\mathbf{p}) \\
&= -N k_B \left(\log 4\pi - \log Z + \Lambda : \left(Q + \tfrac{1}{3} I\right)\right)
\end{aligned} \tag{21}$$

where we have again used the definition of Z and expression for Q to compute the integrals.

Supposing that we may invert (20) – we will do this numerically in section 5 – we have an expression for the free energy in terms of Q. Given that the free energy is a scalar, it is rotationally invariant and so for a uniaxial system ($P = 0$) the free energy should only be a function of the scalar order parameter S. We plot the free energy for three different temperatures in 3b For high temperatures, we see there is one minimum at $S = 0$ which corresponds to an isotropic state. At lower temperatures, there is one minimum at $S > 0$ which corresponds to a (partially) nematically ordered state. At some critical temperature T_C, we see that there are two minima, one at $S = 0$ and one at $S > 0$ at which point the isotropic and nematic phases can coexist. Again, the theory correctly predicts a phase transition, but has far fewer undetermined parameters, and will also be able to handle elastically anisotropic nematic phases.

3   Nonequilibrium dynamics

3.1   Maier-Saupe field theory

To extend the model to the case of nonequilibrium dynamics, we use the field theory presented in [5] and implemented in [6] wherein the order parameter is assumed to be in local equilibrium over a small volume at every point in space. In this case, Λ also becomes a function of position, and the free energy becomes a free energy density which must be integrated over space:

$$f_b(Q, \Lambda) = -\alpha Q : Q + n k_B T \left(\log 4\pi - \log Z + \Lambda : \left(Q + \tfrac{1}{3} I\right)\right) \tag{22}$$

Here we have labeled the free energy density f_b to indicate that it corresponds to a *bulk* free energy, and replaced N with n the number density of molecules.

To account for spatial variation in the order parameter field over the domain, we must introduce elastic terms to the free energy density. The standard way of going about this for a uniaxial nematic with a fixed scalar order parameter S is to write down all possible gradients in the director field up to second order which are invariant under spatial rotations and sign change of the director. The result consists of four terms (supposing molecules are achiral), called the Frank elastic terms. In general, these have four different associated elastic constants K_1, K_2, K_3, K_4 which correspond to splay, twist, bend, and saddle-splay distortions of the director field respectively [2] – see Fig. 4 for a visualization of the first three of these modes.
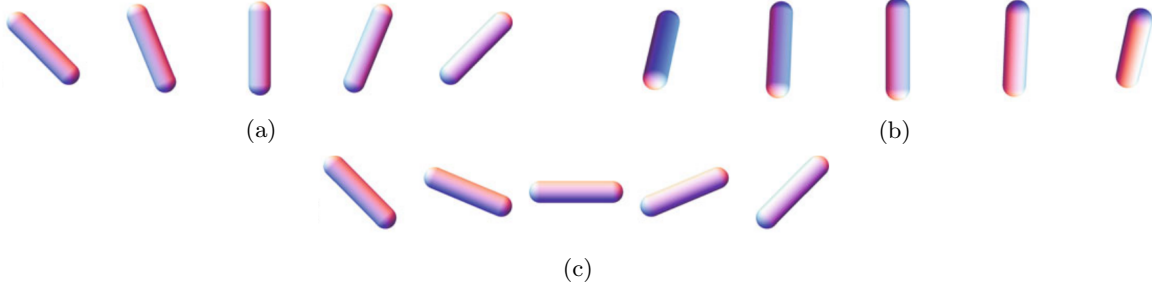

(a)   (b)

(c)

Figure 4: A cartoon of different possible gradients that the director can undergo. In (a) splay, the gradient direction points perpendicular to the main director component, but parallel to the varying component. In (b) twist, the gradient direction points perpendicular to the main director component, and perpendicular to the varying component. In (c) bend, the gradient direction is parallel to the main director component and perpendicular to the varying component. This figure is taken from [2].

It happens that K_4 is a divergence of a field, and so can be reduced to a surface integral by the divergence theorem. For now we fix the configuration at the boundaries (Dirichlet conditions) and so the saddle-splay term is inconsequential for our model.

To extend these terms to a tensor theory, we consider the possible invariants which involve gradients of the Q-tensor, and then use those which reduce to the Frank elastic terms in the case of a uniaxial, constant scalar-order nematic [7]. These are as follows:

$$f_e(\nabla Q) = L_1 \left| \nabla Q \right|^2 + L_2 \left| \nabla \cdot Q \right|^2 + L_3 \nabla Q \vdots \left[(Q \cdot \nabla) Q \right] \tag{23}$$

In index notation this reads:

$$f_e(Q, \nabla Q) = L_1 \left(\partial_k Q_{ij} \right)^2 + L_2 \left(\partial_j Q_{ij} \right)^2 + L_3 Q_{lk} \left(\partial_l Q_{ij} \right) \left(\partial_k Q_{ij} \right) \tag{24}$$

These elastic constants may be written in terms of the Frank elastic constants and the constant scalar order parameter S_0:

$$L_1 = \frac{1}{12 S_0^2} (K_3 - K_1 + 3 K_2)$$

$$L_2 = \frac{1}{2 S_0^2} (K_1 - K_2 - K_4) \tag{25}$$

$$L_3 = \frac{1}{4 S_0^3} (K_3 - K_1)$$

Note that, given the added freedom of a tensorial order parameter to capture nonuniform order and biaxiality, there are much more complicated theories that one may write down in principle.

For our simplified system, the total free energy is then given by an integral of the free energy densities over the domain:

$$F = \int_\Omega f_b(Q) + f_e(Q, \nabla Q) dV = \int_\Omega f(Q, \nabla Q) dV \tag{26}$$

7

Then, for a purely thermodynamically-driven system, the time evolution of the order parameter can be found by taking the negative variation of the free energy with respect to the order parameter:

$$-\delta F = -\int_\Omega \left(\frac{\partial f}{\partial Q} \delta Q + \frac{\partial f}{\partial (\nabla Q)} \delta(\nabla Q) \right) dV$$
$$= -\int_\Omega \left(\frac{\partial f}{\partial Q} - \nabla \cdot \frac{\partial f}{\partial (\nabla Q)} \right) \delta Q \, dV \tag{27}$$

The time evolution of the order parameter field is then the traceless, symmetric part of the factor in parentheses:

$$\frac{\partial Q}{\partial t} = -\frac{\partial f}{\partial Q} + \nabla \cdot \frac{\partial f}{\partial (\nabla Q)} \tag{28}$$

where here a mobility coefficient is set to one. In order to maintain the traceless and symmetric character of Q in the evolution, one may introduce a Lagrange multiplier scheme which adds the following constraints to the free energy:

$$f_l(Q) = \lambda_0 Q : I + \lambda \cdot (\varepsilon : Q) \tag{29}$$

where λ_0 is a scalar Lagrange multiplier enforcing Q be traceless, λ is a vector Lagrange multiplier enforcing Q be symmetric, and ε is the Levi-Civita tensor.

An explicit calculation of the time evolution yields:

$$\frac{\partial Q}{\partial t} = 2\alpha Q - n k_B T \Lambda + 2L_1 \nabla^2 Q \tag{30}$$
$$+ L_2 \left(\nabla (\nabla \cdot Q) + [\nabla (\nabla \cdot Q)]^T - \tfrac{2}{3} (\nabla \cdot (\nabla \cdot Q)) I \right)$$
$$+ L_3 \left(2\nabla \cdot (Q \cdot \nabla Q) - (\nabla Q) : (\nabla Q)^T + \tfrac{1}{3} |\nabla Q|^2 I \right)$$

where we have explicitly solved for the Lagrange multiplier terms λ_0 and λ, and substituted back into the evolution equation. This is the purely thermodynamic time-evolution equation for the order parameter Q.

3.2 Topological defects

Given that the nematic state can spatially vary, the director – the main axis of molecular orientation – is a function of position. Supposing a fixed S value, and letting $\mathbf{n}$ be undefined at certain points, there can be places where $\mathbf{n}$ wraps around points in non-trivial ways as in Fig. 5. These structures can be characterized by the number of rotations that the director makes along a path around the undefined point. That is, for a two-dimensional configuration the director can be characterized by an angle θ that is made with the x-axis so that we may define a so-called "topological charge" m by:

$$\frac{1}{2\pi} \oint_\gamma d\theta = m \tag{31}$$

where γ is some closed loop around the defect.

These are dubbed "topological" because $\theta \circ \gamma$ defines a mapping from $[0, 1]$ into $\mathbb{RP}^1$ (in two dimensions) which may be identified in a purely topological manner with an element of the fundamental group of $\mathbb{RP}^1$ [8]. Note that the appropriate space for the director is $\mathbb{RP}^1$ because we identify $\mathbf{n}$ and $-\mathbf{n}$ in the same way that $\mathbb{RP}^1$ is created by identifying antipodal points of S^1. Additionally, under the isotropic elasticity approximation (see section 3.3) the topological defects feel an effective two-dimensional Coulombic force [2]. It is an active area of research to understand the dynamics of defects under more general conditions.
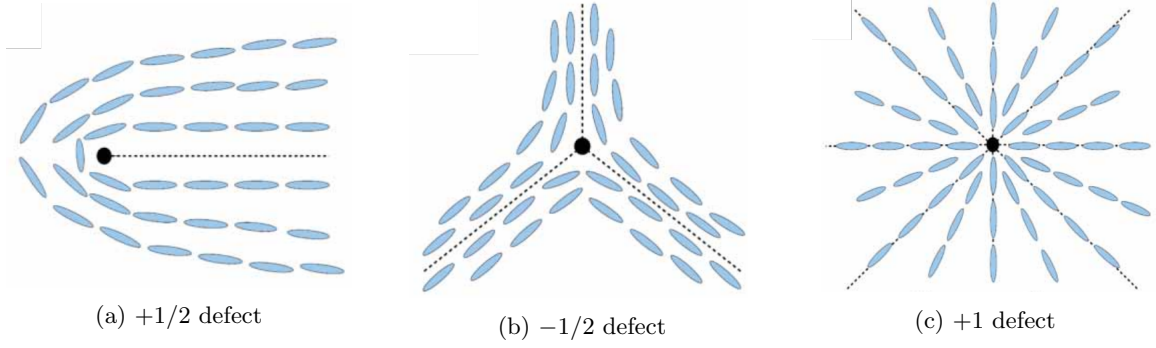
(a) +1/2 defect   (b) −1/2 defect   (c) +1 defect

Figure 5: Schematics of topological defects of various charges. Figure from [9]

3.3 Landau-de Gennes and anisotropic elasticity

A typical approximation that is used when modeling nematic liquid crystals is that elasticity is isotropic: that is, each of the deformation modes shown in Fig. 4 are penalized by the same amount in the free energy. More concretely, $K_1 = K_2 = K_3$ which translates, in the tensorial picture, to $L_2 = L_3 = 0$. However, this is generically not a valid approximation. For example, in an actin-based nematic liquid crystal system, it has been shown that the ratio of bend to splay constants K_3/K_2 can be varied from about 0.5 to 2 by varying the filament length, which drastically changes the defect shape [10]. This poses a problem, because for a fourth order Landau-de Gennes bulk free energy as given in Eq. (8), and an elastic free energy as given by Eq. (23) with $L_3 \neq 0$, the Landau-de Gennes free energy is not bounded below. Hence, there is no global minimizer of the free energy functional.

To illustrate this, we do a short calculation on a simple system. Consider a nonequilibrium Q-configuration given by:

$$Q = (S_0 + \epsilon \sin(kx)) \operatorname{diag}(q_1, q_2, q_3) \tag{32}$$

Here the director points in a fixed direction along the x-, y-, or z-axis dictated by eigenvalues q_1, q_2, q_3, and varies periodically in the scalar order parameter according to S_0, ϵ, and k. Calculating the bulk free energy density yields:

$$
\begin{aligned}
f_b(Q) = (S_0 + \epsilon \sin(kx))^2 \Big[&\tfrac{A}{2} \left(q_1^2 + q_2^2 + q_3^2 \right) \\
&+ \tfrac{B}{3} \left(S_0 + \epsilon \sin(kx) \right) \left(q_1^3 + q_2^3 + q_3^3 \right) \\
&+ \tfrac{C}{4} \left(S_0 + \epsilon \sin(kx) \right)^2 \left(q_1^2 + q_2^2 + q_3^2 \right)^2 \Big]
\end{aligned}
\tag{33}
$$

while the elastic free energy density yields:

$$f_e(Q, \nabla Q) = \left[L_1 + L_3 q_1 \left(S_0 + \epsilon \sin(kx) \right) \right] \epsilon^2 k^2 \left(q_1^2 + q_2^2 + q_3^2 \right) \cos^2(kx) \tag{34}$$

Clearly k does not control the amplitude in Eq. (33), and will thus not affect the total bulk free energy of a configuration, supposing the free energy density is integrated over some integer number of oscillations. However, from Eq. (34) the total elastic free energy is quadratic in k. Hence, so long as we have that:

$$L_3 q_1 (S_0 + \epsilon \sin(kx)) < -L_1 \tag{35}$$

on a majority of the domain, then k can increase without bound to give a total free energy that is arbitrarily negative. This can be accomplished by setting the director along the y-axis so that $q_1 < 0$, and setting S_0 large enough so that the inequality holds. This is simulated via the finite element method in [11], and it is found that the configuration quickly blows up.

Indeed, a more general result is proved in [5] which shows that for a fourth-order Landau-de Gennes free energy and $L_3 \neq 0$, a system with arbitrary Dirichlet boundary conditions can be made to have arbitrarily negative free energy. This is not the case with the singular potential.

9

With this theory, the Lagrange multiplier values Λ diverge to infinity as any of the eigenvalues of Q approach the physically allowed limits. Hence, S_0 is limited by these bounds and so, under appropriate conditions on the elastic constants, one can show that there is a unique minimizer of the singular potential [11]. For this reason, the theory is able to simulate elastic anisotropy, while the standard Landau-de Gennes theory is not.

4 Hydrodynamics

The derivation of the time evolution of the system in the preceding section assumed a system driven purely by free energy minimization. That is, no transfer of mass or corresponding hydrodynamic flow, only transfer of energy and entropy. This is insufficient for many cases, however, as one might imagine flows having a non-negligible effect on molecular alignment [12, 13]. That said, there is yet to be a hydrodynamic theory for the Q-tensor model which is generally accepted by the community. By using general conservation laws of fluid mechanics applied to the director formulation of nematic liquid crystal theory, Ericksen and Leslie were able to derive hydrodynamic equations of a uniaxial nematic liquid crystal system with constant scalar order [3, 14]. However, it happens that for a more general tensorial theory one needs additional contitutive relations in order to produce governing equations.

There have been several attempts at this, including by Beris and Edwards through use of their "dissipation bracket", by Qian and Sheng through methods similar to Ericksen and Leslie but with additional contitutive equations, and by Sonnet and Virga through use of a generalized Rayleigh dissipation function [15, 16, 17]. All of these models are still poorly characterized and so to follow [12] we choose the Qian and Sheng formulation. They, however, use a Landau-de Gennes expression for the bulk portion of their free energy while we use the singular bulk potential presented in Sec. 2.3.

In what follows, we quote the hydrodynamic equations and explain several simplifying assumptions that we make upon a first analysis. We begin with the equation of motion for the Q-tensor:

$$J\ddot{Q} = h + h' \tag{36}$$

Here J is the moment of inertia density (which we will take to be negligible), h is the generalized force from thermodynamics and h' is the viscous generalized force. The generalized force h is given as in section 3 as:

$$h = -\frac{\partial f}{\partial Q} + \nabla \cdot \frac{\partial f}{\partial (\nabla Q)} - \lambda_0 Q : I - \lambda \cdot (\varepsilon : Q) \tag{37}$$

Here we have separated out the Lagrange multipliers λ_0 and λ once again to constrain $\partial Q/\partial t$ to be symmetric and traceless no matter which hydrodynamic terms arise. λ_0 is a scalar, I is the 3×3 identity matrix, λ is a vector, and ε is the Levi-Civita symbol. The viscous generalized force is given by:

$$-h' = \tfrac{1}{2}\mu_2 A + \mu_1 N \tag{38}$$

where $A = \frac{1}{2}\left(\nabla v + (\nabla v)^T\right)$ is the symmetric part of the velocity gradient tensor, and $N = dQ/dt + (WQ - QW)$ is the corotational derivative, representing the time rate of change of Q is a frame that rotates with the fluid element. Here $d/dt = \partial/\partial t + \nabla \cdot v$ is the material derivative, and $W = \frac{1}{2}\left(\nabla v - (\nabla v)^T\right)$ is the antisymmetric part of the velocity gradient tensor. To find an expression for the time evolution of Q we use (38) and (36) to solve for N:

$$N = \frac{1}{\mu_1}h - \frac{1}{2}\frac{\mu_2}{\mu_1}A \tag{39}$$

Here we have assumed J to be negligible so that $J\ddot{Q} \approx 0$ in (36). The definition of N then yields:

$$\frac{dQ}{dt} = \frac{1}{\mu_1}h + [Q, W] - \frac{1}{2}\frac{\mu_2}{\mu_1}A \tag{40}$$

10

with $[Q, W] = QW - WQ$ the commutator.

The generalized Navier-Stokes equation is given by:

$$\rho \frac{dv}{dt} = \nabla \cdot \left(-pI + \sigma^d + \sigma^f + \sigma' \right) \tag{41}$$

with v the velocity, p the pressure, σ^d the stress tensor from distortions in the nematic field, σ^f the stress tensor from external fields (i.e. electric and magnetic), and σ' the viscous stress tensor. This along with the incompressibility condition $\nabla \cdot v = 0$ defines the set of equations. We do not consider external fields so that $\sigma^f = 0$ and we suppose that the velocity field adapts quickly to the nematic configuration as argued in [18] so that $dv/dt \approx 0$. The elastic stress is given in terms of the free energy density as:

$$\sigma^d = -\frac{\partial f}{\partial(\nabla Q)} : (\nabla Q)^T \tag{42}$$

The viscous stress tensor is given by:

$$\sigma' = \beta_1 Q \left(Q : A \right) + \beta_4 A + \beta_5 QA + \beta_6 AQ + \frac{1}{2}\mu_2 N \tag{43}$$
$$- \mu_1 QN + \mu_1 NQ$$

It has been shown that, in configurations of defect annihilation the β_1, β_5, and β_6 terms are negligible, only producing quantitative effects [12]. Additionally, we choose to neglect the μ_1 terms. These do, in fact, produce a qualitative difference in the case of defect annihilation, creating an asymmetry in the trajectory of $+1/2$ and $-1/2$ defects. However, for now we seek to linearize the flow equation so that we only have to solve a much simpler Stoke's system. In the future we seek to include all terms of the viscous stress tensor in the hydrodynamic theory.

These simplifications, along with (39) give the following flow equation:

$$0 = \nabla \cdot \left(-pI + \sigma^d + \beta_4 A + \frac{\mu_2}{2\mu_1} h - \frac{\mu_2^2}{4\mu_1} A \right) \tag{44}$$

Solving for A yields:

$$-2\nabla \cdot A + \frac{1}{\gamma_1}\nabla p = \nabla \cdot \left(\frac{1}{\gamma_1}\sigma^d + \frac{1}{\gamma_2} h \right) \tag{45}$$

with viscosities γ_1 and γ_2 given by:

$$\gamma_1 = \frac{\beta_4}{2} - \frac{\mu_2^2}{8\mu_1}, \quad \gamma_2 = \frac{\mu_1\beta_4}{\mu_2} - \frac{\mu_2}{4} \tag{46}$$

Hence, equations (40) and (45) comprise our coupled hydrodynamic and thermodynamic system. Note that σ^d and h only depend on Q, so that we have (somewhat artificially) decoupled the right-hand side from flow. As a final note, we explicitly calculate σ^d:

$$\sigma^d = -2L_1\nabla Q : (\nabla Q)^T - L_2 \left(\nabla \cdot Q \right) \cdot (\nabla Q)^T - 2L_3 \left(Q \cdot \left[(\nabla Q) : (\nabla Q)^T \right] \right)^T \tag{47}$$

5 Numerical scheme

To solve these equations numerically, we first discretize in time by using a semi-implicit method which leverages convexity of several terms to increase the convergence rate. Given the semi-implicit time-stepping scheme, as well as the nonlinearity of the equations, we must use Newton's method to update the time step. Spatial discretization is done by introducing a weak form of the equations, and then using a finite element method to solve each of the coupled equations. In the course of setting up the finite element system, we will need to compute the Lagrange multiplier Λ and we will also need to find the Jacobian of that mapping, due to the overall Newton's method imposed on the implicit time-stepping scheme. This must be done efficiently, as it happens at every quadrature point in the finite element mesh several times per time-step. We detail each of these steps below.

5.1 Nondimensionalization

We begin by nondimensionalizing the generalized force h, whose explicit expression is exactly the right-hand side of (30). To do this, we introduce a length-scale ξ and write gradients as derivatives with respect to the nondimensional length $\bar{x} = x/\xi$. Additionally, we may divide by the energy density nk_BT:

$$\frac{h}{nk_BT} = \frac{2\alpha}{nk_BT} - \Lambda + \frac{2L_1}{nk_BT\xi^2}\nabla^2 Q \tag{48}$$

$$+ \frac{L_2}{nk_BT\xi^2}\left(\nabla\left(\nabla\cdot Q\right) + \left[\nabla\left(\nabla\cdot Q\right)\right]^T - \tfrac{2}{3}\left(\nabla\cdot\left(\nabla\cdot Q\right)\right)I\right)$$

$$+ \frac{L_3}{nk_BT\xi^2}\left(2\nabla\cdot\left(Q\cdot\nabla Q\right) - \left(\nabla Q\right):\left(\nabla Q\right)^T + \tfrac{1}{3}\left|\nabla Q\right|^2 I\right)$$

Now we define the following quantities:

$$\xi = \sqrt{\frac{2L_1}{nk_BT}}, \quad \overline{\alpha} = \frac{2\alpha}{nk_BT}, \quad \overline{h} = \frac{h}{nk_BT}, \quad \overline{L_2} = \frac{L_2}{L_1}, \quad \overline{L_3} = \frac{L_3}{L_1} \tag{49}$$

Substituting and dropping the overlines for brevity, this yields:

$$h = \alpha Q - \Lambda + \nabla^2 Q + L_2\,E_2(Q,\nabla Q) + L_3\,E_3(Q,\nabla Q) \tag{50}$$

with anisotropic elastic terms given by:

$$E_2(Q,\nabla Q) = \tfrac{1}{2}\left[\nabla\left(\nabla\cdot Q\right) + \left[\nabla\left(\nabla\cdot Q\right)\right]^T\right] - \tfrac{1}{3}\left(\nabla\cdot\left(\nabla\cdot Q\right)\right)I \tag{51}$$

$$E_3(Q,\nabla Q) = \nabla\cdot\left(Q\cdot\nabla Q\right) - \tfrac{1}{2}\left(\nabla Q\right):\left(\nabla Q\right)^T + \tfrac{1}{6}\left|\nabla Q\right|^2 I \tag{52}$$

To nondimensionalize (40), we first note that A and W have dimensions of inverse time, because the characteristic length scale ξ cancels between the gradient and the velocity. Hence, we may introduce a characteristic time τ as:

$$\frac{1}{\tau}\frac{dQ}{d\bar{t}} = \frac{nk_BT}{\mu_1}\overline{h} + \frac{1}{\tau}[Q,\overline{W}] - \frac{1}{2}\frac{\mu_2}{\mu_1}\frac{1}{\tau}\overline{A} \tag{53}$$

Given this, we make the following definitions:

$$\tau = \frac{\mu_1}{nk_BT}, \quad \gamma = -\frac{1}{2}\frac{\mu_2}{\mu_1} \tag{54}$$

Note that μ_2/μ_1 is typically negative so that the so-called flow-alignment parameter γ is positive. Dropping overlines, this gives:

$$\frac{dQ}{dt} = h + [Q,W] + \gamma A \tag{55}$$

For the Stokes equation, we begin by nondimensionalizing the elastic stress tensor. Substituting the characteristic length, we end up with:

$$\overline{\sigma}^d = -\nabla Q : \left(\nabla Q\right)^T - \tfrac{1}{2}\overline{L}_2\left(\nabla\cdot Q\right)\cdot\left(\nabla Q\right)^T - \overline{L}_3\left(Q\cdot\left[\left(\nabla Q\right):\left(\nabla Q\right)^T\right]\right) \tag{56}$$

with:

$$\sigma^d = \overline{\sigma}^d nk_BT \tag{57}$$

With this, the flow equation reads:

$$-2\frac{1}{\tau\xi}\nabla\cdot A + \frac{1}{\gamma_1}\frac{\eta}{\xi}\nabla p = \frac{1}{\xi}\nabla\cdot\left(\frac{1}{\gamma_1}nk_BT\sigma^d + \frac{1}{\gamma_2}nk_BTh\right) \tag{58}$$

Here η is a dimensional parameter associated with p. Multiplying through by $\xi\tau$, and then using the definition of τ we find:

$$-2\nabla \cdot A + \nabla p = \nabla \cdot \left(\zeta_1 \sigma^d + \zeta_2 h\right) \tag{59}$$

where we have taken:

$$\eta = \gamma_1/\tau, \quad \zeta_1 = \left(\frac{1}{2}\frac{\beta_4}{\mu_1} - \frac{1}{8}\left(\frac{\mu_2}{\mu_1}\right)^2\right)^{-1}, \quad \zeta_2 = \left(\frac{\beta_4}{\mu_2} - \frac{1}{4}\frac{\mu_2}{\mu_1}\right)^{-1} \tag{60}$$

Hence, the remaining parameters in the system are: the interaction parameter α which is controlled by the temperature; the anisotropic elasticities L_2 and L_3; the flow-alignment parameter γ which controls the nematic's tendency to align along the direction of flow; and the two viscosity parameters ζ_1 and ζ_2 which control the relative weight with which generalized force and elastic stress tensor affect the flow configuration.

5.2 Discretization of Q-tensor equation

Given that the Q-tensor is tracless and symmetric, we may write it in terms of its degrees of freedom as:

$$Q = \begin{bmatrix} Q_1 & Q_2 & Q_3 \\ Q_2 & Q_4 & Q_5 \\ Q_3 & Q_5 & -(Q_1 + Q_4) \end{bmatrix} \tag{61}$$

and collect those degrees of freedom into a five-component vector, q:

$$q = \begin{bmatrix} Q_1 \\ Q_2 \\ Q_3 \\ Q_4 \\ Q_5 \end{bmatrix} \tag{62}$$

There are several other traceless and symmetric quantities which are functions of Q (and therefore may be written as vector functions of q), but which require tensor contraction operations, and can thus not simply be notated as vector operations on q. In an attempt to compartmentalize cumbersome notation, we collect the degrees of freedom of these traceless, symmetric tensors into corresponding vectors, and write them as functions of the vector q to write:

$$\Lambda(Q) \to \lambda(q), \quad E_2(Q, \nabla Q) \to e_2(q, \nabla q), \quad E_3(Q, \nabla Q) \to e_3(q, \nabla q), \quad [Q, W] \to c(q), \quad A \to a \tag{63}$$

These may be calculated explicitly by writing Q as in (61), calculating the tensorial terms, and then taking the appropriate entries to construct a vector as in (62). For the time evolution of q, these expressions will be written explicitly in terms of the degrees of freedom Q_i.

To discretize in time we first note that in Eq. (12) $-TS$ is convex while $\langle E \rangle = -\alpha Q : Q$ is concave [11]. The free energy is then a difference between a convex part and a concave part, which is referred to as a convex splitting [19]. For systems governed by such a free energy, it happens that treating the convex part implicitly and the concave part explicitly can make the scheme unconditionally energy-stable, and guarantee convergence in Newton's method regardless of the initial guess. We do that here, also treating the elastic and hydrodynamic terms implicitly.

$$\frac{q - q_0}{\delta t} + v \cdot \nabla q = \alpha q_0 - \lambda(q) + \nabla^2 q + L_2\, e_2(q, \nabla q) + L_3\, e_3(q, \nabla q) + c(q) + \gamma a \tag{64}$$

where q is the configuration at the current time-step, q_0 is the configuration at the previous time-step, and δt is the step size. Given that this is a nonlinear equation which we seek to solve via

a finite element method, we must use the Newton-Rhapson method to linearize. To that end, we define a vector residual:

$$\mathcal{R}(q^n) = q^n + v \cdot \nabla q^n - (1 + \delta t\, \alpha)q_0 - \delta t\left(-\lambda(q^n) + \nabla^2 q^n + L_2\, e_2(q^n, \nabla q^n) + L_3\, e_3(q^n, \nabla q^n) + c(q^n) + \gamma a\right) \tag{65}$$

where q^n is the value of q for the nth Newton iteration. Then the iterative method reads:

$$\mathcal{R}'(q^n)\delta q^n = -\mathcal{R}(q^n)$$
$$q^{n+1} = q^n + \alpha_0 \delta q^n \tag{66}$$

with $\mathcal{R}'$ the Gateaux derivative of the residual, and δq^n the variation of q which must be solved for at each time step. $\alpha_0 < 1$ is a step size that can be made smaller for a system for which the convergence is more sensitive. Explicitly, the Jacobian $\mathcal{R}'$ reads:

$$\mathcal{R}'\delta q^n = \delta q^n + v \cdot \nabla \delta q^n - \delta t\left[-\left(\frac{\partial \lambda}{\partial q}\right)\bigg|_{q^n} \delta q^n + \nabla^2 \delta q^n \right. \tag{67}$$
$$\left. + L_2 e_2'(q^n, \nabla q^n)\,\delta q^n + L_3 e_3'(q^n, \nabla q^n)\,\delta q^n + c'(q^n)\,\delta q^n\right]$$

Here e_2' and e_3' are linear operators which depend on the configuration at the last Newton iteration, and contain differential operators. c' is a matrix whose values only depend on q^n.

We now cast this linear equation in its weak form by taking an inner product with an arbitrary (vector) test function φ:

$$\langle \varphi, \mathcal{R}'\delta q\rangle = -\langle \varphi, \mathcal{R}\rangle \tag{68}$$

where here we define the inner product as:

$$\langle f, g\rangle = \int_\Omega f \cdot g \tag{69}$$

for the domain Ω. To recast this as a discrete problem, we dictate that (68) must be satisfied for some finite-dimensional subspace of the space of test functions with basis ϕ_i. Further, we represent the solution δq^n (approximately) as a linear combination of these basis elements:

$$\delta q^n = \sum_i \delta q_i^n \varphi_i \tag{70}$$

Using (70) with (68) and integrating by parts yields an equation with the following form:

$$A_{ij}^n \delta q_j^n = b_i^n \tag{71}$$

with

$$A_{ij}^n = \langle \varphi_i, \varphi_j\rangle + \langle \varphi_i, v \cdot \nabla \varphi_j\rangle - \delta t\left[-\left\langle \varphi_i, \left(\frac{\partial \lambda}{\partial q}\right)\varphi_j\right\rangle - \langle \nabla \varphi_i, \nabla \varphi_j\rangle \right. \tag{72}$$
$$\left. + L_2\langle \varphi_i, e_2'\varphi_j\rangle + L_3\langle \varphi_i, e_3'\varphi_j\rangle + \langle \varphi_i, c'\varphi_j\rangle\right]$$

and

$$b_i = \langle \varphi_i, q^n\rangle + \langle \varphi_i, v \cdot \nabla q^n\rangle - (1 + \delta t\, \alpha)\langle \varphi_i, q_0\rangle \tag{73}$$
$$- \delta t\left[-\langle \varphi_i, \lambda(q^n)\rangle - \langle \nabla \varphi_i, \nabla q^n\rangle + L_2\langle \varphi_i, e_2(q^n)\rangle \right.$$
$$\left. + L_3\langle \varphi_i, e_3(q^n)\rangle + \langle \varphi_i, c(q^n)\rangle + \gamma\langle \varphi_i, a(v)\rangle\right]$$

Here we have, for the isotropic elasticity terms, integrated by parts:

$$\langle \varphi_i, \nabla^2 \varphi_j\rangle = \langle \varphi_i, n \cdot \nabla \varphi_j\rangle_{\partial\Omega} + \langle \nabla \varphi_i, \nabla \varphi_j\rangle \tag{74}$$

where n is the unit vector normal to the boundary $\partial\Omega$, and the corresponding inner product is integrated over the boundary. For now we assume either Dirichlet or zero-valued Neumann conditions. In the former case, the test functions φ_i come from the space tangent to the solution space so that they are zero on the boundary. In the latter case, the normal derivative is zero. In both cases, the boundary term vanishes. For more general boundary-conditions (nonzero Neumann or mixed), we just end up with another term on the right-hand side which can be calculated from the values of the normal derivative prescribed at the boundary.

5.3 Discretization of the Stokes equation

Given that the simplified hydrodynamic model gives the flow velocity in the form of a typical Stoke's equation, the discretization is somewhat standard. We first collect the equations into a single vector equation:

$$\begin{pmatrix} -2\nabla \cdot A(v) + \nabla p \\ -\nabla \cdot v \end{pmatrix} = \begin{pmatrix} \nabla \cdot \left(\zeta_1 \sigma^d + \zeta_2 h \right) \\ 0 \end{pmatrix} \tag{75}$$

We then dot with a vector set of test equations $\begin{pmatrix} u & q \end{pmatrix}^T$ with u in the space of velocity functions, and q in the space of pressure functions. This yields:

$$\langle u, -2\nabla \cdot A(v) + \nabla p \rangle - \langle q, \nabla \cdot v \rangle = \langle u, \nabla \cdot \left(\zeta_1 \sigma^d + \zeta_2 h \right) \rangle \tag{76}$$

Now we may use the divergence theorem to integrate by parts, and also note that:

$$\begin{aligned} \tfrac{1}{2} \left(\nabla u \right) : \left(\nabla v + (\nabla v)^T \right) &= \tfrac{1}{2} \left(\partial_i u_j \right) \left(\partial_j v_i + \partial_i v_j \right) \\ &= \tfrac{1}{4} \left[\left(\partial_i u_j \right) \left(\partial_j v_i + \partial_i v_j \right) + \left(\partial_j u_i \right) \left(\partial_i v_j + \partial_j v_i \right) \right] \\ &= A(u) : A(v) \end{aligned} \tag{77}$$

where for the second term in the second equality we have relabeled $i \rightarrow j$, $j \rightarrow i$. Given this, the weak form of our equation reads:

$$2\langle A(u), A(v) \rangle - \langle \nabla \cdot u, p \rangle - \langle q, \nabla \cdot v \rangle = -\langle \nabla u, \zeta_1 \sigma^d + \zeta_2 h \rangle \tag{78}$$

Here we have chosen no slip boundary conditions so that the boundary terms from the weak form go to zero.

To discretize, we choose a finite element basis $\varphi_i = \begin{pmatrix} \varphi_{i,v} & \varphi_{i,p} \end{pmatrix}$ to act as our test functions as well as a basis for our solution. The equations in the form above constitute a symmetric saddle-point problem, as defined in terms of bilinear forms on the spaces of velocity and pressure functions. It happens that, in order for the solution to the discretized problem to be stable (e.g. not contain artifacts such as spurious oscillations), the finite-dimensional solution space must satisfy the Ladyzhenskaya-Babuska-Brezzi (LBB) condition, which is a constraint on $\langle \nabla \cdot u, p \rangle$ restricted to the finite element space [20]. We omit the details here, but for our purposes it suffices to choose Lagrange (piece-wise polynomial) elements so that the pressure part of the solution $\varphi_{i,p}$ is represented by elements of degree d, and the velocity solution $\varphi_{i,v}$ is represented by elements of degree $d+1$. This then becomes a matrix inversion problem with matrix

$$A_{ij} = 2\langle A(\varphi_{i,v}), A(\varphi_{j,v}) \rangle - \langle \nabla \cdot \varphi_{i,v}, \varphi_{j,p} \rangle - \langle \varphi_{i,p}, \nabla \cdot \varphi_{j,v} \rangle \tag{79}$$

and right-hand side:

$$b_i = -\langle \nabla \varphi_{i,v}, \zeta_1 \sigma^d + \zeta_2 h \rangle \tag{80}$$

5.4 Algorithm details

To initialize the system, we project a nematic configuration onto the finite element solution space of the q-vector. This configuration typically is some arrangement of topological defects. We then

iterate forward in time several steps ($\sim 20\,\tau$) to let it relax before introducing hydrodynamics. We do this because the analytic expressions for topological defects typically only dictate the director angle at each point in space, and so there is a singularity at the defect cores, resulting in large gradients and therefore large velocity fields. By letting the (largely diffusive) system relax, the scalar order parameter S decreases near the defect cores so that the Q-tensor configuration is smoother. As explained above, to step in time we must iterate a Newton-Rhapson equation until some tolerance is reached for the norm of the residual (65). For the initial configuration, we fix $v = 0$.

Once the system is initialized and relaxed, we introduce hydrodynamics. Given that we are solving two simultaneous equations, we iterate in time as follows: the first Newton iteration of the Q-configuration q^1 is solved using the velocity field v^0 from the last time step. Then we solve for the velocity field v^1 corresponding to q^1. Given v^1 we may solve for the q-configuration at the next Newton iteration, q^2. We continue back and forth until the residual $\mathcal{R}$ reaches some tolerance. Given that the dependence of v on q is not taken into account when computing the Jacobian of the residual $\mathcal{R}'$, it is necessary to take a much smaller step for each Newton iteration: we choose $\alpha_0 = \frac{1}{2}$.

To solve the matrix equation for δq, we use an iterative GMRES solver [21]. An iterative solver is preferable over a direct solver in order to save on memory costs, as well as operation scaling: for GMRES, only vector-vector and matrix-vector operations are necessary so that, for a sparse matrix as in this problem, each iteration scales linearly with the number of degrees of freedom. Additionally, in a problem simulating only diffusion (no hydrodynamics) we have implemented the BoomerAMG algebraic multigrid solver to precondition the matrices [22]. This method has the added benefit of keeping the number of GMRES iterations constant so that the entire solver scales linearly. Further, both of these solvers can run in a distributed fashion so that the program can be parallelized to thousands of processors.

To solve the Stoke's equation, we borrow largely from [23]. Here they use a Schur complement method to decouple the velocity and pressure equations into two symmetric matrix equations. The matrix equation is then solved by using a mix of direct solvers, and iterative Conjugate Gradient solvers [21]. See [23] for details. Note also that the algebraic multigrid method can be used as a preconditioner for this system, thus allowing it to be highly scalable via parallelization.

This algorithm is implemented in $C++$ using the deal.II finite element library for the standard steps: mesh-generation, finite element basis functions, projection onto finite element space, building finite element matrices, distributing boundary constraints, solving matrix inversion problems, and several other operations [24, 25]. The project is open source and freely available at [26].

To underscore the scalability of the algorithm, we provide strong and weak scaling of a simulation of a single defect for a purely diffusive system ($v = 0$) with isotropic elasticity in Fig. 6. These tests were run on the Expanse supercomputer, a part of the San Diego Supercomputing Center [27] using highly parallelized software from the Portable, Extensible Toolkit for Scientific Computation (PETSc) [28, 29, 30], and the p4est parallel adaptive mesh refinement library [31]. Note that all of the trends follow the ideal linear scaling quite closely. The divergence from linear scaling in both the weak and strong scaling cases can be explained by there not being not enough workload for each individual processor (i.e. too many processors, or too few degrees of freedom).

5.5   Inverting the Lagrange multiplier function

For each iteration of Newton's method as described in section 5.4, we must numerically calculate both the Lagrange multiplier λ_i, as well as its Jacobian $\partial \lambda_i / \partial q_i$. We do this by using a Newton-Rhapson method as well, with a residual given by (see (20)):

$$R_i = \frac{\int_{S^2} (p_{r(i)} p_{c(i)} - \frac{1}{3}\delta_{r(i)c(i)}) \exp(p_k p_l \Lambda_{kl}) dS(\mathbf{p})}{\int_{S^2} \exp(p_k p_l \Lambda_{kl}) dS(\mathbf{p})} - q_i \tag{81}$$
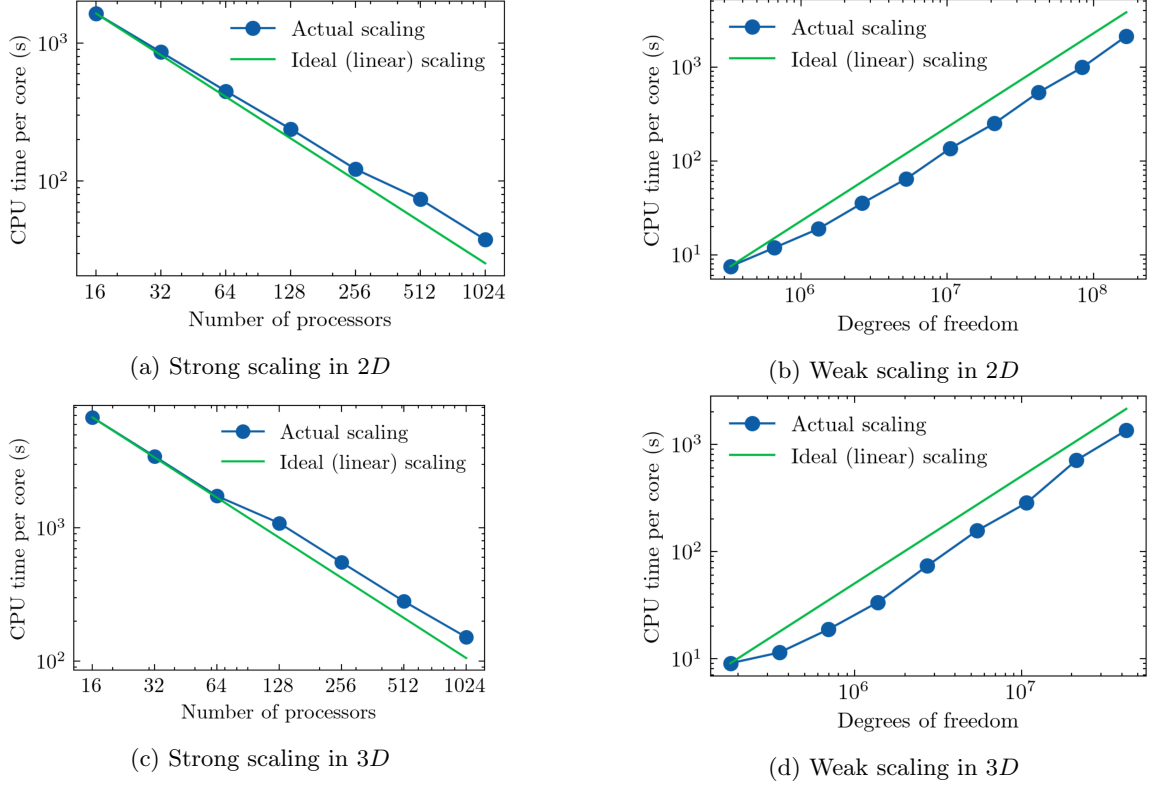
(a) Strong scaling in $2D$

(b) Weak scaling in $2D$

(c) Strong scaling in $3D$

(d) Weak scaling in $3D$

Figure 6: Strong and weak scaling of defect relaxation simulations in $2D$ and $3D$ plotted logarithmically. In (a) there are ~ 5 million degrees of freedom, and in (c) there are ~ 10 million degrees of freedom. Both (b) and (d) are run on 512 CPU cores.

where here we use $r(i)$ and $c(i)$ to refer to the row and column respectively in the Q-tensor where the ith degree of freedom is found. Given that there are five entries of R_i, we must already compute $5+1$ integrals via quadrature. Additionally, in computing the 5×5 Jacobian matrix $R'_{ij} = \partial R_i / \partial \lambda_j$ to iterate Newton's method, it happens that one must compute two new integrals around the sphere per entry, resulting in an additional 50 integrals. Even with a method specifically designed for integrals over the sphere, such as Lebedev Quadrature, this operation becomes the dominant computational cost in the code [32, 33].

To circumvent this, we first note that Q and Λ can be simultaneously diagonalized [11]. For a diagonalized traceless tensor there are only two degrees of freedom, and so the corresponding residual is two components and its Jacobian is a 2×2 matrix. This corresponds to a total of six integrals around the sphere. Hence, we may first diagonalize Q and record the corresponding rotation matrix, compute the two degrees of freedom of the diagonalized Λ-tensor, and then find Λ in the original frame by computing the inverse rotation. However, we also seek to calculate $\partial \lambda / \partial q$. In the case described above, where we calculate the full five degrees of freedom with Newton's method, that quantity is just the inverse of the residual's Jacobian. For this, we construct a commutative diagram of the relevant mappings in Fig. 7.

Here ϕ maps the degrees of freedom of the traceless, symmetric tensors to entries in a vector in $\mathbb{R}^5$, diag is the diagonalization procedure which is unique on the space of symmetric matrices, ψ maps the degrees of freedom of the diagonalized traceless, symmetric tensors to $\mathbb{R}^2$ and degrees of freedom of rotation matrices to $\mathbb{R}^5$ via some means. For numerical stability we use unit quaternions to represent the rotations, keeping in mind that it does not matter that they double-cover $SO(3)$ so long as we consistently map to a single half. Additionally, Λ is the mapping which takes the Q-tensor to its unique Lagrange multiplier, and λ is the same for the vector representation. Given
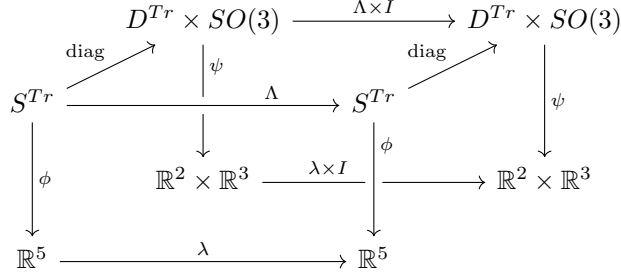
17

Figure 7: A commutative diagram of mappings relevant to inverting $Q(\Lambda)$

all this, we may write λ as:

$$\lambda = \left(\phi \circ \mathrm{diag}^{-1} \circ \psi^{-1}\right) \circ (\lambda \times I) \circ \left(\psi \circ \mathrm{diag} \circ \phi^{-1}\right) \tag{82}$$

Each mapping in parentheses is just a mapping on $\mathbb{R}^5$ and so we may compute them numerically. The chain rule then gives:

$$d\lambda = d\left(\phi \circ \mathrm{diag}^{-1} \circ \psi^{-1}\right) \cdot (d\lambda \times I) \cdot d\left(\psi \circ \mathrm{diag} \circ \phi^{-1}\right) \tag{83}$$

Hence, to find the Jacobian of λ it suffices to find the Jacobians of the diagonalizing and inverse diagonalizing mappings, as well as the Jacobian of λ in the reduced case.

It is not possible to find a closed analytic expression for the diagonalization of a 3×3 matrix which is numerically stable, and so we cannot compute a Jacobian for these mappings analytically. However, automatic differentiation affords us a way to compute the derivatives of these mappings using one of the many numerically-stable diagonalization schemes, such as the Jacobi method, or the QL method with implicit shifts [34, 35, 36]. Computing the derivatives only adds a small factor (roughly two here) to the number of computations. Finally, diagonalizing these matrices introduces further symmetry into the spherical integrals since only factors of x^2, y^2 and z^2 appear. In this case we only need to integrate over the positive octant, which reduces the number of quadrature points by another factor of eight.

6 Comparison with previous results

6.1 Verification of rotational diffusion without hydrodynamics

As a first test for the code, we verify the relaxation of a prototypical configuration with previously published results. For simplicity, we choose an isotropic system ($L_2 = L_3 = 0$) without hydrodynamics $v = 0$ in a quasi-two-dimensional domain. That is, the director is allowed to point in any direction in three dimensions, but we restrict the configuration to be uniform in the third dimension. This is a typical assumption for thin film experiments. The nematic configuration is a $+1/2$ defect with scalar order parameter $S = 0.6715$. Explicitly, the initial Q-tensor field reads:

$$Q = \frac{S}{2} \begin{bmatrix} \frac{1}{3} + \cos(\theta) & \sin(\theta) & 0 \\ \sin(\theta) & \frac{1}{3} - \cos(\theta) & 0 \\ 0 & 0 & -\frac{2}{3} \end{bmatrix} \tag{84}$$

where θ is the polar coordinate angle. The boundaries of the domain are fixed at these values (i.e. we use Dirichlet conditions). The system size is $\frac{10}{\sqrt{2}} \times \frac{10}{\sqrt{2}}$ in units of the characteristic length ξ (see section 5.1), and the finite element mesh is a 256×256 gridpoint square composed of quadrilaterals. To relax the system, we have run Newton's method to make $\partial q/\partial t \approx 0$, though we could have just

as easily iterated in time via the semi-implicit method until the system does not change appreciably between time steps. Indeed, this is what the code in [11] does, which should give the same relaxed configuration. One other difference between the simulation presented here and the reference code is that the latter uses triangles for cells, and hence uses a somewhat different mesh.
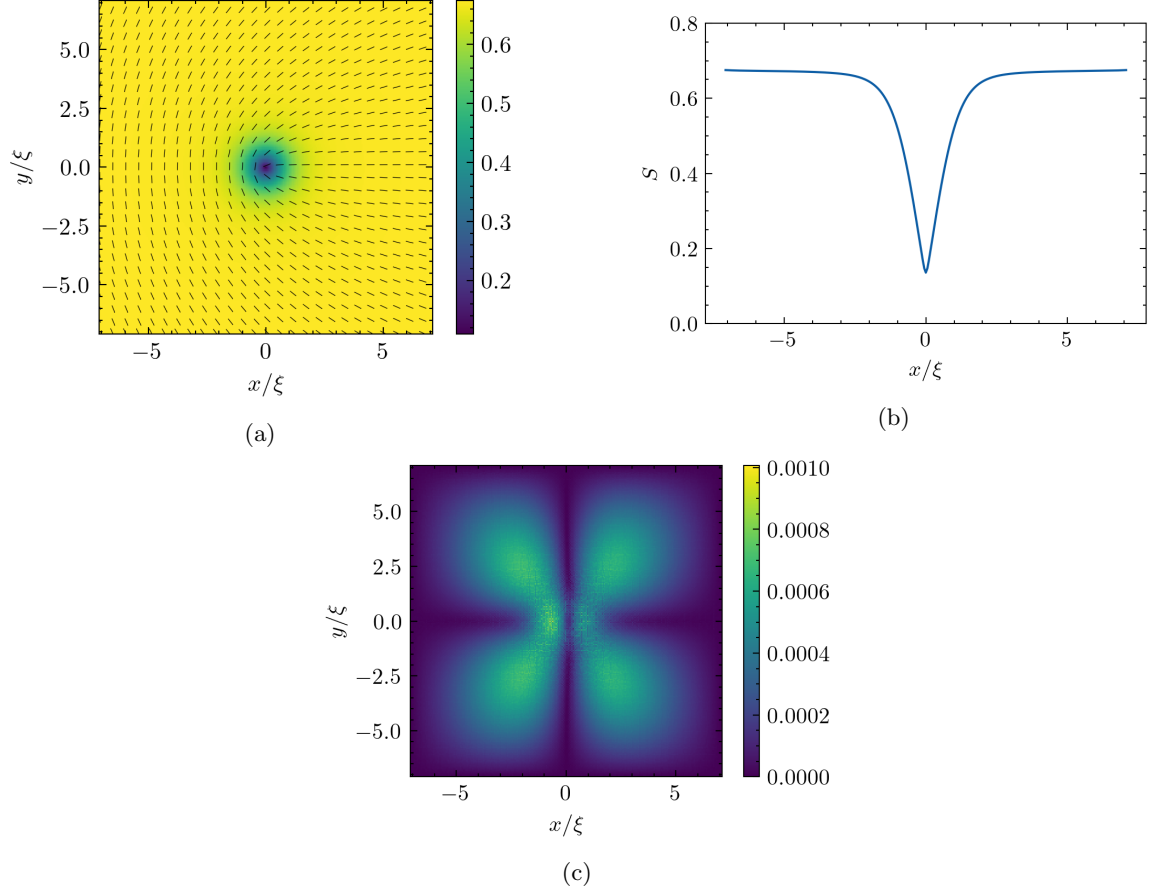

(a)

(b)

(c)

Figure 8: Results from the relaxation of a +1/2 defect. Here (a) is a plot of the defect with dashes representing the director orientation and color scheme representing the scalar order parameter S, (b) is a cross-section of S horizontally through the middle of the defect, and (c) is the vector norm of the difference between the calculated configuration and a reference configuration produced by code from [11] $|q - q_{\text{ref}}|$.

The configuration is shown in 8a with a cross-section of the scalar order parameter S through the defect shown in 8b. As expected, S is symmetric about the center, and the defect sizing is on the order of the characteristic length. Further, in the defect core S decreases linearly until it reaches the center [37].

As a final check we can plot the vector norm of the difference between this configuration and one generated by code used in [11]. In 8c we see take the fluctuations in the center to be numerical noise, given that they happen on the order of pixels. Further, the maximal difference is approximately 1% of the total vector norm. Given the different discretizations of the problem (simplices vs quadrilaterals) we take this to be a confirmation of the efficacy of the program.

6.2 Verification of hydrodynamics

To verify the hydrodynamic component of the code, we consider a two-dimensional system comprising one $+1/2$ and one $-1/2$ defect pointing away from one another, as in 9a. We may then – after having relaxed the configuration as described in section 5.4 – calculate the hydrodynamic flows arising from each of the terms in (59) and compare them to the flows found in [18]. Note that, during the configuration relaxation we force $v = 0$ so that backflows do not inform the nematic configuration which produce the flows in Fig. 10. Although not explicitly stated, we understand this to be the case for the reference flow configurations as well.

Once again we take the isotropic elasticity approximation because the flows that we are interested in comparing to use a Landau-de Gennes free energy, and thus are restricted to the isotropic approximation. The system size here is $\frac{1,400}{3} \times \frac{1,400}{3}$ in units of ξ with outer mesh size 256×256 grid points. The defects, themselves a distance $70\,\xi$ apart, live in a central region of size $\frac{280}{3} \times \frac{280}{3}$ in units of ξ. In the central region, the grid-spacing is half of what it is on the rest of the domain so that the nematic and flow configurations near the defects can be better-resolved. In all of the plots that follow, only the central region is shown.

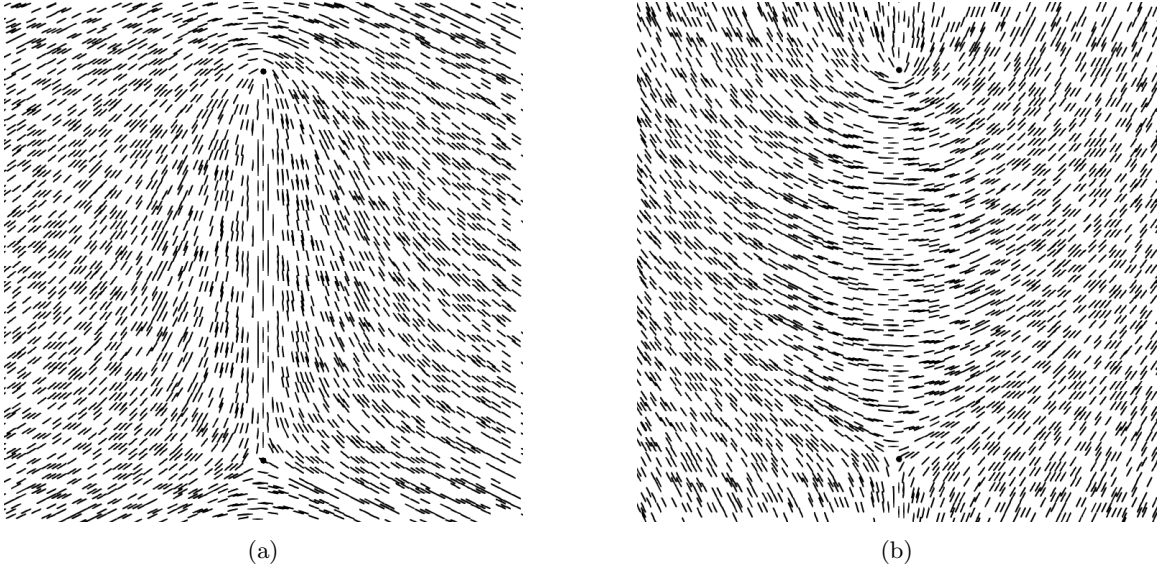(a)   (b)

Figure 9: Schematic representation of the two-defect configurations, with dashes corresponding to the nematic-director angle at that point. These two isomorphs differ by a $\pi/2$ global director rotation, and so any term in the free energy invariant under that transformation treats these configurations identically. Note that (a) corresponds to the defects pointing *away* from one another (the $+1/2$ defect moves like a comet) and (b) corresponds to the defects pointing *towards* one another.

For these preliminary results from the linearized hydrodynamic equations (44), there are three contributions from the nematic configuration to the flow: the β_4 and μ_2 viscosity terms, as well as the terms arising from the elastic stress tensor σ^d. To qualitatively compare with [18] we keep the β_4 term, and then separately consider flows arising from the μ_2, and σ^d terms. More concretely, we solve (59) for the two-defect configuration given in Fig. 9a including separate contributions from each term ζ_1 and ζ_2 on the right-hand side.

In Fig. 10b and 10e, we note that both configurations contain four vortices, and that the flow direction is such that the defects are pushed toward one another. The vortex centers in our configuration are further from the center of the domain, likely due to different bulk free energy parameters or to the difference in definition of the characteristic length. Additionally, the configuration is symmetric about the two defects. This can be understood, as described in [18], by the transformation which turns the $+1/2$ and $-1/2$ defects into one another $Q_{xy} \rightarrow -Q_{xy}$. Because

(a) all terms   (b) elastic term   (c) μ_2 term

(d) all terms, reference configuration   (e) elastic terms, reference configuration   (f) μ_2 terms, reference configuration
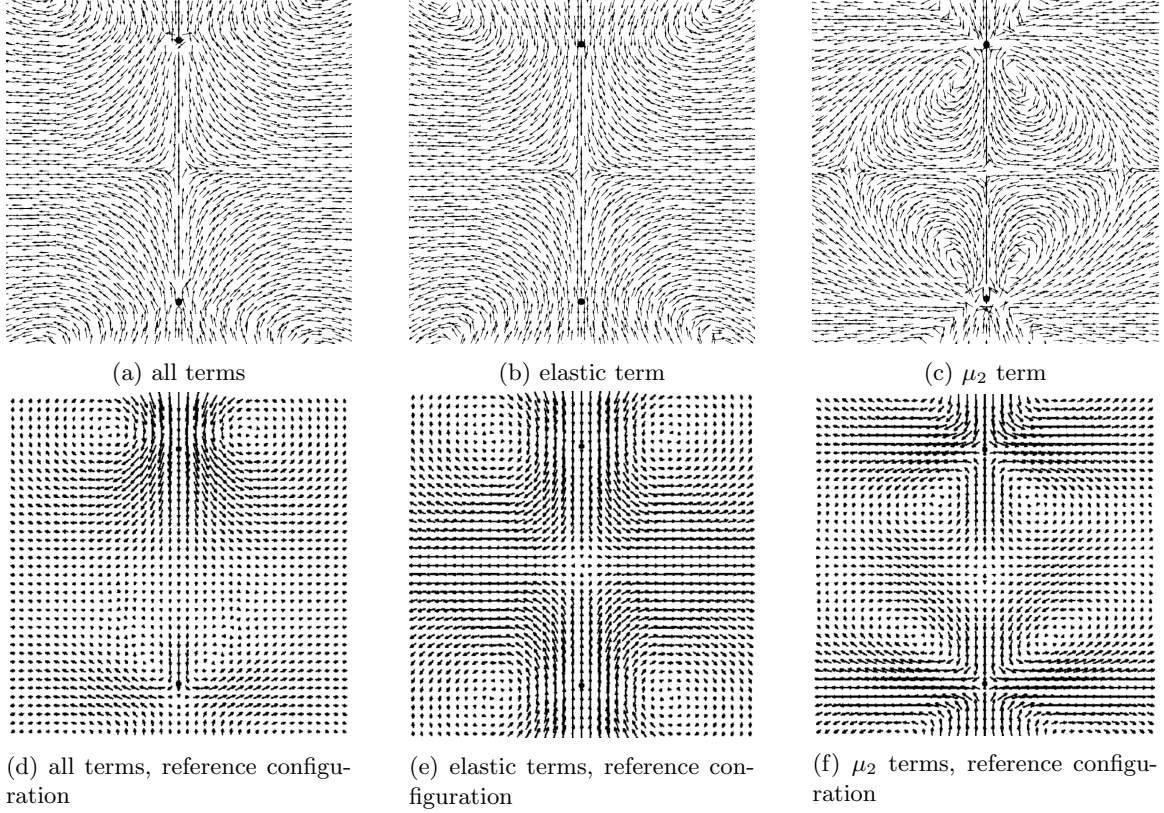
Figure 10: Instantaneous flow configurations arising from the nematic configuration pictured in 9a. Figures (a)-(c) are our velocity fields produced by solving (59), while (d)-(e) are reference configurations from [18], in which they solve (41) with viscous stress tensor (43). Figure (b) considers only the σ^d elastic term, (c) considers only the h term which corresponds to the μ_2 viscous contribution, and (a) contains both. Figure (e) considers only elastic terms, (f) considers μ_2 terms, while (d) considers elastic and all of the viscous terms described in (43). Note that all of the configurations consider the β_4 viscous term. Additionally, (a)-(c) only contain the directions of the velocity field, while (d)-(e) give the magnitude as the arrow length.

the isotropic elastic stress tensor is insensitive to this change, the resulting flow configuration is symmetric between the two.

The flow in Fig. 10c, by contrast, is not symmetric about the defects, and in fact the transformation described above has no definite symmetry properties with respect to N. As a result, there is a slight asymmetry in the shape of the vortices around each defect. In any case, we see six vortices instead of four, moving in directions that are consistent with Zumer's results.

Finally, we notice significant differences between the flow configurations in Fig. 10a and those in Fig. 10d. This is due to the fact that we have neglected the μ_1 viscous terms which, at the location of the $+1/2$ defect point *toward* the $-1/2$ defect, and and at the location of the $-1/2$ defect point *away* from the $+1/2$ defect. Thus, at the $-1/2$ defect location the flows from the μ_1 viscous term and the elastic stress tensor cancel out, giving a large asymmetry in the flow velocities at each of the defects. In our case, the elastic flow configuration largely dominates and so the total flow configuration only has four vortices.

7 Proposed research

The main objective of this project is to develop a theory which can describe the dynamics of nematic liquid crystals through the use of the Q-tensor order parameter, accounting for hydrodynamics as well as anisotropic elasticity. In the course of developing this theory, we are also creating a corresponding finite element algorithm and open source implementation in the C++ programming language capable of simulating such systems, including full three dimensional configurations.

Our motivation for using the Q-tensor is two-fold: for simulations which use a director approach with fixed scalar order parameter S, the director is undefined at the center of defects. Hence, to treat defects one typically has to cut out the defect core and assign some energy, introducing potentially arbitrary parameters of defect radius and defect energy. Even considering a variable scalar order parameter, the energy associated with three-dimensional line defects diverges and so these must also be treated carefully, analogous to the method above. For the Q-tensor approach, its values and gradients remain well-defined even at defect cores, giving a way to resolve structures inaccessible to the director approach. This becomes especially important in lyotropic liquid crystals, in which defect cores can become large and complex structures. These systems arise in many emerging applications of active and biological matter.

In addition to these practical considerations, the director approach is only able to accommodate uniaxial nematic configurations. The Q-tensor, by contrast, is able to accommodate biaxiality. While typically unimportant for uniform configurations, biaxiality is thought to be present in defect cores which could affect defect dynamics. Additionally, interactions with the substrate are thought to induce strong biaxiality. Hence, for a full picture of non-uniform nematic configurations it is necessary to use the full Q-tensor formalism.

Our model is also able to accommodate anisotropic elasticity. This is important because in certain lyotropic chromonic liquid crystals, the elastic constants differ by an order of magnitude or more, making the isotropic approximation unjustified [38]. Additionally, while the elastic constants of active and biological systems remain poorly characterized, it is likely that they are highly anisotropic. In particular, it has been found that in lyotropic liquid crystals composed of filamentous actin the ratio between the bend and splay constants K_3/K_1 can be tuned from about 1/2 to 2 by changing the average length of the actin filaments, and by a sparse addition of rigid microtubule filaments [39]. These ratios are estimated based on the shape of the resulting 1/2 defects which vary from very U-shaped in the case of high splay-constant systems, to very V-shaped in the case of high bend-constant systems. Based on the same morphological differences it is known that nematic activity due to motor proteins can effectively lower the bend constant K_1 [40]. It is expected that this altered defect morphology affects defect dynamics in a nontrivial way. To explore this role, we will use our theory to simulate several different classes of systems.

7.1 Backflows in quasi-two dimensional systems from defects

In the classical work by Svensek and Zumer referenced above, they investigate the effect of backflows on the trajectories of two defects of opposite charge [12]. However, they use a Landau-de Gennes bulk free energy and are thus limited to the single-constant isotropic elasticity approximation. We seek to investigate a similar system, but with anisotropy between the splay and bend elastic modes.

In their investigation, they consider two isomorphs, one in which the the defects are pointing towards each other, and one away as in Fig. 9a and 9b respectively. For isotropic elasticity, the free energy is unaffected by a rotation of the director by some fixed phase everywhere in space. A rotation by $\pi/2$ turns one isomorph into the other, and so the defect motion should be the same in either case. However, given that the region in between the defects in isomorph (a) is dominated by splay, while the region between the defects in isomorph (b) is dominated by bend, it is expected that anisotropy will cause different annihilation trajectories between the two scenarios. Additionally, for isotropic elasticity the two defects experience symmetric, parabolic-in-time trajectories and annihilate in the

center of their initial separation. This is because, as mentioned in section 6.2, the $Q_{xy} \rightarrow -Q_{xy}$ transformation turns one into the other. Given that anisotropic elasticity causes the defects to locally relax into different shapes – U-like for splay-dominated, V-like for bend-dominated – this symmetry no longer holds and so we expect the trajectories to be asymmetric.

Extending beyond two defects, in the isotropic case without backflows the time evolution of two dimensional defected configurations is harmonic, and so multiple-defect configurations are just additive. Indeed, such configurations may be understood as a polar Coulomb gas. However, for anisotropic systems the lowest order energy is nonlinear and so the presence of additional defects is expected to affect defect morphology and dynamics in a nontrivial way. One potential route of study is in understanding the statistics of many defects in these anisotropic, quasi-2D systems.

7.2 Three-dimensional configurations

In three dimensions, instead of only point defects we may additionally find line-defects. For the simplest case, a so-called wedge disclination may be constructed by taking a two-dimensional defect like those shown in Fig. 5 and extending it to be uniform in the third dimension. However, in this case the directors may point in the third dimension and so for a purely $+1/2$ defect manufactured as described, along a plane perpendicular to the defect line one may continuously rotate the director field to a twist defect, and then to a $-1/2$ defect. Hence, there is no purely topological difference between $+1/2$ and $-1/2$ defects in three dimensions. Given this, there is some question as to whether there is a persistent asymmetry in the backflows produced by wedge disclinations as demonstrated by [12] in two dimensions. In recent measurements it has been shown that pairs of disclinations do follow the same parabolic-in-time annihilation pattern shown in [12] in the case without backflow, and so it is speculated that the wedge defects undergo the transformation described above so that they both become twist defects [41]. This is true no matter the defect configuration (straight and parallel vs. curved more generally), though certain theories predict it should only be true for straight disclinations [42]. It has been argued that the mechanism for transformation into twist disclinations could be explained by the system having a much smaller twist constant than bend or splay. We will use our computational scheme to investigate the role that the ratio of bend-splay to twist elastic constants plays in restoring the symmetry of these defect annihilations.

As another example of a fully three-dimensional system that we can investigate, active nematics driven by motor proteins have been observed to spontaneously generate and annihilate loop defects [43, 44]. As such, these systems are generically unstable, and evolve into a turbulent state. The loops which are created have zero topological charge, and thus may only involve pure-twist geometries, or may involve wedge-twist geometries. Given that there are mixtures of geometries which are characterized by different elastic modes, the dynamics of single defects and interactions between defects depend sensitively on anisotropy.

7.3 Kinematic law for defect evolution

Using methods introduced to study superfluid vortices, an exact kinematic law for nematic disclinations in three dimensions has been derived [45]. This law is rather general, in that it can include any nematodynamics including hydrodynamic transport. Hence, this law is compatible with our fully hydrodynamic theory and so we may numerically explore different cases in which the law gives unexpected results. One instance is in the case of two defects oriented orthogonal to one another in two dimensions in which, for topological reasons, the defects move diagonally from one another before annihilating [46]. It is expected that such nonintuitive scenarios will arise in the case of line and loop defects in three dimensions. We will be able to use our theory to understand the interactions between hydrodynamic backflow, anisotropic elasticity, and kinematics such as these driven by topological charge conservation.

References

[1] Wikimedia Commons, "Cholesteryl benzoate," 2007.

[2] J. V. Selinger, *Introduction to the Theory of Soft Matter: From Ideal Gases to Liquid Crystals.* Soft and Biological Matter, Cham: Springer International Publishing, 2016.

[3] J. L. Ericksen, "Hydrostatic theory of liquid crystals," *Archive for Rational Mechanics and Analysis*, vol. 9, pp. 371–378, Jan. 1962.

[4] J. L. Ericksen, "Liquid crystals with variable degree of orientation," *Archive for Rational Mechanics and Analysis*, vol. 113, no. 2, pp. 97–120, 1991.

[5] J. M. Ball and A. Majumdar, "Nematic Liquid Crystals: From Maier-Saupe to a Continuum Theory," *Molecular Crystals and Liquid Crystals*, vol. 525, pp. 1–11, July 2010.

[6] C. D. Schimming and J. Viñals, "Computational molecular field theory for nematic liquid crystals," *Physical Review E*, vol. 101, p. 032702, Mar. 2020.

[7] N. J. Mottram and C. J. P. Newton, "Introduction to Q-tensor theory," *arXiv:1409.3542 [cond-mat]*, Sept. 2014. arXiv: 1409.3542.

[8] N. D. Mermin, "The topological theory of defects in ordered media," *Reviews of Modern Physics*, vol. 51, pp. 591–648, July 1979.

[9] G. Foffano, J. Lintuvuori, A. Tiribocchi, and D. Marenduzzo, "The dynamics of colloidal intrusions in liquid crystals: a simulation perspective," *Liquid Crystals Reviews*, vol. 2, pp. 1–27, Jan. 2014.

[10] R. Zhang, N. Kumar, J. L. Ross, M. L. Gardel, and J. J. de Pablo, "Interplay of structure, elasticity, and dynamics in actin-based nematic materials," *Proceedings of the National Academy of Sciences*, vol. 115, Jan. 2018.

[11] C. D. Schimming, J. Viñals, and S. W. Walker, "Numerical method for the equilibrium configurations of a Maier-Saupe bulk potential in a Q-tensor model of an anisotropic nematic liquid crystal," *Journal of Computational Physics*, vol. 441, p. 110441, Sept. 2021.

[12] D. Svenšek and S. Žumer, "Hydrodynamics of pair-annihilating disclination lines in nematic liquid crystals," *Physical Review E*, vol. 66, p. 021712, Aug. 2002.

[13] G. Tóth, C. Denniston, and J. M. Yeomans, "Hydrodynamics of Topological Defects in Nematic Liquid Crystals," *Physical Review Letters*, vol. 88, p. 105504, Feb. 2002.

[14] F. M. Leslie, "Some constitutive equations for liquid crystals," *Archive for Rational Mechanics and Analysis*, vol. 28, pp. 265–283, Jan 1968.

[15] A. N. Beris and B. J. Edwards, *Thermodynamics of Flowing Systems: with Internal Microstructure.* Oxford Engineering Science Series, New York: Oxford University Press, 1994.

[16] T. Qian and P. Sheng, "Generalized hydrodynamic equations for nematic liquid crystals," *Physical Review E*, vol. 58, pp. 7475–7485, Dec. 1998.

[17] A. M. Sonnet and E. G. Virga, *Dissipative Ordered Fluids.* Boston, MA: Springer US, 2012.

[18] D. Svenšek and S. Žumer, "Complex backflow dynamics in nematic liquid crystals," *Continuum Mechanics and Thermodynamics*, vol. 14, pp. 231–239, June 2002.

[19] J. Xu, Y. Li, S. Wu, and A. Bousquet, "On the stability and accuracy of partially and fully implicit schemes for phase field modeling," *Computer Methods in Applied Mechanics and Engineering*, vol. 345, pp. 826–853, Mar. 2019.

[20] D. Boffi, F. Brezzi, and M. Fortin, *Mixed Finite Element Methods and Applications*, vol. 44 of *Springer Series in Computational Mathematics*. Berlin, Heidelberg: Springer Berlin Heidelberg, 2013.

[21] J. W. Demmel, *Applied numerical linear algebra*. Philadelphia: Society for Industrial and Applied Mathematics, 1997.

[22] V. E. Henson and U. M. Yang, "BoomerAMG: a Parallel Algebraic Multigrid Solver and Preconditioner," *Applied Numerical Mathematics*, vol. 41, no. 5, pp. 155–177, 2002.

[23] M. Kronbichler and W. Bangerth, "Deal.ii step-22 tutorial program," 2022.

[24] D. Arndt, W. Bangerth, B. Blais, M. Fehling, R. Gassmöller, T. Heister, L. Heltai, U. Köcher, M. Kronbichler, M. Maier, P. Munch, J.-P. Pelteret, S. Proell, K. Simon, B. Turcksin, D. Wells, and J. Zhang, "The `deal.II` library, version 9.3," *Journal of Numerical Mathematics*, vol. 29, no. 3, pp. 171–186, 2021.

[25] D. Arndt, W. Bangerth, D. Davydov, T. Heister, L. Heltai, M. Kronbichler, M. Maier, J.-P. Pelteret, B. Turcksin, and D. Wells, "The deal.II finite element library: Design, features, and insights," *Computers & Mathematics with Applications*, vol. 81, pp. 407–422, 2021.

[26] L. Myers, "maier-saupe-lc-hydrodynamics." `https://github.com/lucasmyers97/maier-saupe-lc-hydrodynamics`, 3 2022.

[27] S. Strande, H. Cai, M. Tatineni, W. Pfeiffer, C. Irving, A. Majumdar, D. Mishin, R. Sinkovits, M. Norman, N. Wolter, T. Cooper, I. Altintas, M. Kandes, I. Perez, M. Shantharam, M. Thomas, S. Sivagnanam, and T. Hutton, "Expanse: Computing without Boundaries: Architecture, Deployment, and Early Operations Experiences of a Supercomputer Designed for the Rapid Evolution in Science and Engineering," in *Practice and Experience in Advanced Research Computing*, (Boston MA USA), pp. 1–4, ACM, July 2021.

[28] S. Balay, S. Abhyankar, M. F. Adams, S. Benson, J. Brown, P. Brune, K. Buschelman, E. M. Constantinescu, L. Dalcin, A. Dener, V. Eijkhout, W. D. Gropp, V. Hapla, T. Isaac, P. Jolivet, D. Karpeev, D. Kaushik, M. G. Knepley, F. Kong, S. Kruger, D. A. May, L. C. McInnes, R. T. Mills, L. Mitchell, T. Munson, J. E. Roman, K. Rupp, P. Sanan, J. Sarich, B. F. Smith, S. Zampini, H. Zhang, H. Zhang, and J. Zhang, "PETSc Web page." `https://petsc.org/`, 2022.

[29] S. Balay, S. Abhyankar, M. F. Adams, S. Benson, J. Brown, P. Brune, K. Buschelman, E. Constantinescu, L. Dalcin, A. Dener, V. Eijkhout, W. D. Gropp, V. Hapla, T. Isaac, P. Jolivet, D. Karpeev, D. Kaushik, M. G. Knepley, F. Kong, S. Kruger, D. A. May, L. C. McInnes, R. T. Mills, L. Mitchell, T. Munson, J. E. Roman, K. Rupp, P. Sanan, J. Sarich, B. F. Smith, S. Zampini, H. Zhang, H. Zhang, and J. Zhang, "PETSc/TAO users manual," Tech. Rep. ANL-21/39 - Revision 3.17, Argonne National Laboratory, 2022.

[30] S. Balay, W. D. Gropp, L. C. McInnes, and B. F. Smith, "Efficient management of parallelism in object oriented numerical software libraries," in *Modern Software Tools in Scientific Computing* (E. Arge, A. M. Bruaset, and H. P. Langtangen, eds.), pp. 163–202, Birkhäuser Press, 1997.

[31] C. Burstedde, L. C. Wilcox, and O. Ghattas, "`p4est`: Scalable algorithms for parallel adaptive mesh refinement on forests of octrees," *SIAM Journal on Scientific Computing*, vol. 33, no. 3, pp. 1103–1133, 2011.

[32] "Quadrature rules for the unit sphere." `https://people.math.sc.edu/Burkardt/cpp_src/sphere_lebedev_rule/sphere_lebedev_rule.html`. Accessed: 2022-03-08.

[33] V. Lebedev, "Quadratures on a sphere," *USSR Computational Mathematics and Mathematical Physics*, vol. 16, no. 2, pp. 10–24, 1976.

[34] J. Kopp, "Efficient numerical diagonalization of hermitian 3x3 matrices," *International Journal of Modern Physics C*, vol. 19, no. 3, pp. 523–548, 2008.

[35] The Trilinos Project Team, *The Trilinos Project Website*, 2020 (acccessed May 22, 2020).

[36] The Sacado Project Team, *The Sacado Project Website*, 2022 (acccessed May 5, 2022).

[37] J. Rønning, M. C. Marchetti, M. J. Bowick, and L. Angheluta, "Flow around topological defects in active nematic films," *arXiv:2111.08537 [cond-mat]*, Nov. 2021. arXiv: 2111.08537.

[38] S. Zhou, Y. A. Nastishin, M. M. Omelchenko, L. Tortora, V. G. Nazarenko, O. P. Boiko, T. Ostapenko, T. Hu, C. C. Almasan, S. N. Sprunt, J. T. Gleeson, and O. D. Lavrentovich, "Elasticity of Lyotropic Chromonic Liquid Crystals Probed by Director Reorientation in a Magnetic Field," *Physical Review Letters*, vol. 109, p. 037801, July 2012.

[39] R. Zhang, N. Kumar, J. L. Ross, M. L. Gardel, and J. J. de Pablo, "Interplay of structure, elasticity, and dynamics in actin-based nematic materials," *Proceedings of the National Academy of Sciences*, vol. 115, pp. E124–E133, Jan. 2018.

[40] N. Kumar, R. Zhang, J. J. de Pablo, and M. L. Gardel, "Tunable structure and dynamics of active liquid crystals," *Science Advances*, vol. 4, p. eaat7779, Oct. 2018.

[41] Y. Zushi and K. A. Takeuchi, "Scaling and Spontaneous Symmetry Restoring in Reconnecting Nematic Disclinations," *arXiv:2110.00442 [cond-mat]*, Oct. 2021. arXiv: 2110.00442.

[42] C. Long, X. Tang, R. L. B. Selinger, and J. V. Selinger, "Geometry and mechanics of disclination lines in 3d nematic liquid crystals," *Soft Matter*, vol. 17, pp. 2265–2278, 2021.

[43] G. Duclos, R. Adkins, D. Banerjee, M. S. E. Peterson, M. Varghese, I. Kolvin, A. Baskaran, R. A. Pelcovits, T. R. Powers, A. Baskaran, F. Toschi, M. F. Hagan, S. J. Streichan, V. Vitelli, D. A. Beller, and Z. Dogic, "Topological structure and dynamics of three-dimensional active nematics," *Science*, vol. 367, no. 6482, pp. 1120–1124, 2020.

[44] J. Binysh, i. c. v. Kos, S. Čopar, M. Ravnik, and G. P. Alexander, "Three-dimensional active defect loops," *Phys. Rev. Lett.*, vol. 124, p. 088001, Feb 2020.

[45] C. D. Schimming and J. Viñals, "Singularity identification for the characterization of topology, geometry, and motion of nematic disclination lines," *Soft Matter*, vol. 18, pp. 2234–2244, 2022.

[46] X. Tang and J. V. Selinger, "Orientation of topological defects in 2d nematic liquid crystals," *Soft Matter*, vol. 13, pp. 5481–5490, 2017.